separations

MDPI

Article

Development of the VARICOL Process for the Resolution of Racemic Menthol

Linhe Sun [1,2], Ying Yang [1,2,*] and Jianguo Yu [1,2,*]

[1] National Engineering Research Center for Integrated Utilization of Salt Lake Resources, East China University of Science and Technology, 130 Meilong Road, Shanghai 200237, China
[2] Engineering Research Center of Resources Process Engineering, Ministry of Education, East China University of Science and Technology, 130 Meilong Road, Shanghai 200237, China
* Correspondence: yyang@ecust.edu.cn (Y.Y.); jgyu@ecust.edu.cn (J.Y.); Tel./Fax: +86-21-64252170 (Y.Y. & J.Y.)

Abstract

This paper reports the chiral separation of menthol enantiomers using the VARICOL process to improve productivity. Amylose 3,5-dimethylphenylcarbamate coated on silica gel was employed as the chiral stationary phase, and n-hexane/2-propanol (95/5, v/v) was used as the eluent. To design and optimize the VARICOL process, a linear driving-force model was developed to predict the separation performance. Separation regions of the conventional simulated moving bed (SMB) and VARICOL processes were evaluated and compared. It was found that, under an outlet purity requirement of 95.0%, the five-column VARICOL process has a separation region comparable to that of the six-column conventional SMB process. As an illustrative example, a five-column VARICOL unit and a six-column conventional SMB unit, both operating under the same conditions, were employed to resolve the menthol racemate. Purities for both the extract and raffinate were above 95.0%, and a productivity of 0.400 $g_{racemate}/(L_{CSP}\cdot min)$ and a solvent consumption of 0.355 $L/g_{racemate}$ were achieved in the VARICOL process. Productivity increased by 20% while solvent consumption maintained relative to the conventional SMB process, though product purities decreased slightly.

Keywords: l-menthol; chiral separation; simulated moving bed; VARICOL; mathematical model

1. Introduction

l-menthol, a naturally occurring cyclic monoterpene alcohol [1], is recognized as one of the most important flavors currently [2]. As estimated recently, its global production is more than 34,000 metric tons [3], and its demand is still increasing. It is widely used in candies, chewing gums, cigarettes, cosmetics and pharmaceuticals [4,5]. l-menthol contains three chiral centers in its molecular structure, which leads to seven other optical isomers, including d-menthol, d,l-isomenthol, d,l-neomenthol and d,l-neoisomenthol, as shown in Figure 1. These isomers display an unpleasant smell and are less effective for inducing the cooling sensation when applied to the body's skin [2,3]. Though d,l-menthol is also marketed since it shows no toxicity [6,7], it is less desirable than l-menthol.

As a natural product, l-menthol is present in mint with almost absolute optical purity [1]. In the past, isolation from corn mint oil was the only approach for the production of l-menthol [3]. The price of l-menthol fluctuates violently due to the surging demand and unstable yield. This has promoted the development in synthesis of optically pure l-menthol. Approximately 60% of the l-menthol in the end-use market is derived from

Academic Editor: Petr Bednar

Received: 15 February 2026
Revised: 14 March 2026
Accepted: 16 March 2026
Published: 17 March 2026

chemical synthesis at present [3]. Symrise, Takasago and BASF are the main suppliers of synthetic l-menthol in the world [3,4].

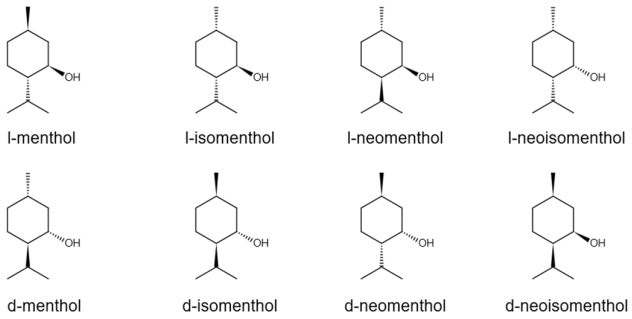

Figure 1. Molecular structure of the menthol optical isomers.

The Symrise process uses thymol as the starting material. A mixture of the four racemic pairs, containing approximately 60% d,l-menthol, 26% d,l-neomenthol, 12% d,l-isomenthol and 2% d,l-neoisomenthol, is obtained by hydrogenation of thymol [8]. l-menthol is subsequently isolated from this mixture after a series of achiral and chiral separation procedures. Achiral separation gives d,l-menthol by distillation, followed by chiral separation of d,l-menthol using the preferential crystallization method to give enantiomerically pure l-menthol as the final product. In the chiral separation process, d,l-menthol is first esterified to give d,l-menthylbenzoate. The racemic esters are then resolved by seeding optically pure ester crystals into the supersaturated solution of d,l-menthylbenzoate. Finally, d-menthol and l-menthol are obtained after hydrolysis [9]. d-menthol, along with the other three racemates, is recycled to the hydrogenation section to re-establish the thermodynamic equilibrium [8]. The enantio-separation of racemic menthol is complex, comprising esterification, enantioselective crystallization and hydrolysis. The esterification is essential because enantiomerically pure d-menthol and l-menthol can not be obtained simply by seeding in racemic menthol solutions [3]. Moreover, the operating conditions of preferential crystallization should be strictly controlled. Enzymatic catalysis may be an alternative strategy for the chiral separation of racemic menthol [10–14].

Chromatography is a promising technique for chiral separation [15–19], with simulated moving bed (SMB) as its continuous form [20,21]. Several fixed beds packed with adsorbent particles are connected in series in an SMB unit, with four inlet and outlet lines, eluent, feed, raffinate and extract, connected between the columns. With periodical switching of these inlet and outlet lines in the direction of fluid flow in this technique, the countercurrent contact of the fluid and adsorbent particles in the true moving bed (TMB) concept is achieved to reinforce the mass transfer. Higher productivity and less solvent consumption compared with batch chromatography make it an attractive method used in sugar refinement [22,23], medicine manufacturing [24–26] and biological production purifications [27–29] since firstly proposed by Universal Oil Products (UOP) in 1961.

A variety of non-conventional modes of SMB were proposed to further improve the performance of SMB [30,31], including Varicol [32–34], Modicon [35,36], Powerfeed [37,38], partial-discard [39,40], outlet stream fractionation and feed-back [41,42], and solvent gradient [43,44]. Among these variants, Varicol was proposed and industrialized by NOVASEP. Figure 2 compares the difference between conventional SMB and VARICOL in operation mode by taking a specific shifting scheme as an example. For both conventional SMB and VARICOL, packed columns located between different inlet and outlet lines have different functions in separation, and thus can be divided into four zones. Zone I is located between the eluent line and the extract line, and is responsible for the regeneration of the stationary phase. Zone II is located between the extract line and the feed line, and is responsible for

the purification of the more-adsorbed component. Zone III is located between the feed line and the raffinate line, and is responsible for the purification of the less-adsorbed component. Zone IV is located between the raffinate line and the eluent line, and is responsible for the regeneration of the mobile phase. Conventional SMB and VARICOL have the same position of inlet and outlet lines, and thereby, the same initial column configurations. In the conventional SMB process, all the inlet and outlet ports shift in the direction of fluid flow for a column simultaneously every particular time interval, namely a switching period. The column configuration remains constant as 1/2/2/1 during the operation. In contrast, in a VARICOL process, the inlet and outlet ports shift asynchronously. The period is further divided into subintervals by these individual shifting, and the column configuration varies within a period. After a quarter of a period as the first subinterval, the extract line shifts downstream for a column, with the column configuration changing into 2/1/2/1. Subsequently, after a quarter of a period as the second subinterval, the feed line shifts downstream for a column, with the column configuration changing into 2/2/1/1. Then, after a quarter of a period as the third subinterval, the eluent line shifts downstream for a column, with the column configuration changing into 1/2/1/2. Finally, after a quarter of a period as the fourth subinterval, the raffinate line shifts downstream for a column, with the column configuration changing back into 1/2/2/1. With this shifting scheme, VARICOL process has an average column configuration of 1.5/1.75/1.5/1.25.

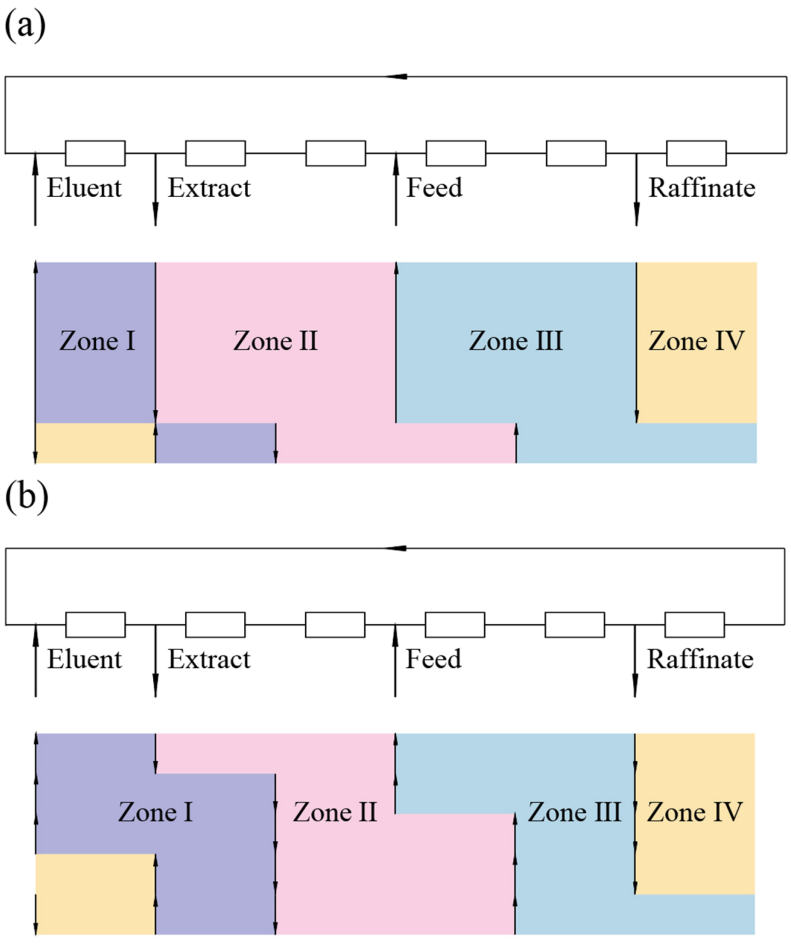

Figure 2. Schematic diagram of ports shifting in (**a**) conventional SMB and (**b**) VARICOL processes.

The asynchronous shifting of the inlet and outlet ports offers a greater degree of freedom for the operation of the VARICOL process. Consequently, with the same column numbers, the VARICOL process can achieve better separation performance than the conven-

tional SMB process under suitable design. This also gives rise to a possibility of achieving the same purities for extract and raffinate with a reduced number of columns using the VARICOL process [32,45,46]. SMB separation process with fewer columns is beneficial for the following reasons [20]. First of all, fewer fixed beds, tubes and valves are used for the equipment setup, and therefore, less device cost and extra-column dead volume. Moreover, a smaller amount of adsorbent is required, especially for chiral separation, because of the high price of the chiral stationary phase. In addition, fewer packing and re-packing efforts are essential. Packed columns should have equivalent hydrodynamic characteristics to ensure symmetry. However, the packing procedure can be irreproducible. Therefore, the packing procedure is always very tedious and time-consuming, and re-packing should be performed for the columns with poor reproductivity.

In our previous work, the conventional simulated moving bed technique was used for the resolution of menthol racemate, and menthol enantiomers with purity above 99.0% can be obtained [47]. Considering the high demand for l-menthol, improving the productivity of the SMB unit is of great importance. This work aims to explore the potential of the VARICOL process for the enantioseparation of the racemic menthol at a reduced product purity target, taking into account the diverse application purposes of l-menthol. Amylose 3,5-dimethylphenylcarbamate coated on silica gel was used as the chiral stationary phase, with n-hexane/2-propanol (95/5, v/v) serving as the mobile phase. Mathematical models were developed to describe the dynamics of the VARICOL process, where mass transfer resistance and axial dispersion were taken into account. The separation regions of the VARICOL processes were estimated by simulations. The superiority of the VARICOL process in terms of separation performance compared with conventional SMB was investigated. Experiments were carried out for the resolution of racemic menthol by conventional SMB and VARICOL process respectively, and the predicted separation performance was compared with the experimental results.

2. Theoretical Analysis

2.1. Mathematical Models of the VARICOL Process

Mathematical modeling is an effective approach for the understanding and design of the SMB separation process. The SMB process can be modeled by two strategies: the TMB strategy and the SMB strategy [22,48]. The first one makes an analogy between the SMB and TMB processes, considering the movement of the solid phase in the opposite direction of the liquid phase [25,49,50]. The steady state of the TMB operation is predicted by a set of ordinary differential equations. The second one describes the real intermittent behavior of the SMB process, considering the periodical shifting of the injection and collection lines [51,52]. The cyclic steady state of the SMB operation is predicted by a set of partial differential equations. Less computation time is required for the TMB strategy, yet acceptable prediction results can be obtained by the TMB strategy only when the column numbers in each zone are at least two, because of the great deviation between the SMB process and TMB process with low total column numbers [53]. The SMB strategy is used in this paper because the total column numbers considered in the current work are five or six. Mass transfer and axial dispersion are taken into account in the model, which contains the following equations [52,54].

Mass balance over a volume element in the liquid phase is as follows:

$$\frac{\partial c_{i,k}}{\partial t} + \frac{u_k}{\varepsilon}\frac{\partial c_{i,k}}{\partial z} + \frac{1-\varepsilon}{\varepsilon}\frac{6}{d_p}K\left(q^*_{i,k} - q_{i,k}\right) = D_{ax,k}\frac{\partial^2 c_{i,k}}{\partial z^2} \quad (1)$$

Mass balance over a volume element in the solid phase is as follows:

$$\frac{\partial q_{i,k}}{\partial t} = \frac{6}{d_p} K\left(q^*_{i,k} - q_{i,k}\right) \tag{2}$$

where the subscript i (i = 1, 2) refers to the species in the racemate, with 1 and 2 representing the less-retained and more-retained enantiomers, d-menthol and l-menthol, respectively, and the subscript k (k = 1, 2, …, N_C) refers to the column number. N_C is the total column number. $c_{i,k}$ and $q_{i,k}$ are the concentrations in the liquid phase and solid phase, respectively. $q^*_{i,k}$ is the saturated solid phase concentration corresponding to the liquid phase concentration. ε is the bulk porosity of the fixed bed. u_k is the superficial velocity. $D_{ax,k}$ is the axial dispersion coefficient. K is the overall mass transfer coefficient. d_p is the particle diameter of the chiral stationary phase. z is the axial coordination of the SMB column. t is the time variable.

The binary adsorption isotherm of the menthol enantiomer can be described by the modified linear + Langmuir model [47].

$$q^*_i = H_i c_i + \frac{Q_{max} b_i c_i}{1 + \sum_{i=1}^{2} b_i c_i} \tag{3}$$

where H_i is the Henry parameter for the linear adsorption site, while Q_{max} and b_i are the Langmuir parameters for the non-linear adsorption site.

The superficial velocity is as follows:

$$u_k = \frac{Q_j}{\frac{\pi}{4} d_C^2} \tag{4}$$

where the subscript j (j = I, II, III, IV) refers to the zone number in the VARICOL unit. Q_j is the flow rate in the packed bed. d_C is the column diameter.

The axial dispersion can be estimated by the Peclet number:

$$Pe = \frac{u_k L_C}{\varepsilon D_{ax,k}} \tag{5}$$

where Pe is the Peclet number, which is a dimensionless number. L_C is the column length.

Initial conditions for the partial differential equations are as follows:

$$c_{i,k}\big|_{t=0,z} = 0 \tag{6}$$

$$q_{i,k}\big|_{t=0,z} = 0 \tag{7}$$

Boundary conditions for the partial differential equations are as follows:

$$D_{ax,k}\left(\frac{\partial c_{i,k}}{\partial z}\right)\Big|_{t,z=0} = \frac{u_k}{\varepsilon}\left(c_{i,k}\big|_{t,z=0} - c_{i,k,in}\right) \tag{8}$$

$$\left(\frac{\partial c_{i,k}}{\partial z}\right)\Big|_{t,z=L_C} = 0 \tag{9}$$

where $c_{i,k,in}$ is the inlet concentration of the packed bed.

Mass balance between two connected columns is given for different cases.

When no stream enters or exits between the two columns,

$$c_{i,k+1,in} = c_{i,k}\big|_{t,z=L_C} \tag{10}$$

When only one stream enters or exits between the two columns,
For the eluent node,

$$Q_{\mathrm{I}} = Q_{\mathrm{IV}} + Q_{\mathrm{D}} \tag{11}$$

$$c_{i,k+1,\mathrm{in}} = \frac{Q_{\mathrm{IV}}}{Q_{\mathrm{I}}} c_{i,k}\big|_{t,z=L_{\mathrm{C}}} \tag{12}$$

For the extract node,

$$Q_{\mathrm{II}} = Q_{\mathrm{I}} - Q_{\mathrm{X}} \tag{13}$$

$$c_{i,k+1,\mathrm{in}} = c_{i,k}\big|_{t,z=L_{\mathrm{C}}} \tag{14}$$

$$c_{i,\mathrm{X}} = c_{i,k}\big|_{t,z=L_{\mathrm{C}}} \tag{15}$$

For the feed node,

$$Q_{\mathrm{III}} = Q_{\mathrm{II}} + Q_{\mathrm{F}} \tag{16}$$

$$c_{i,k+1,\mathrm{in}} = \frac{Q_{\mathrm{II}}}{Q_{\mathrm{III}}} c_{i,k}\big|_{t,z=L_{\mathrm{C}}} + \frac{Q_{\mathrm{F}}}{Q_{\mathrm{III}}} c_{i,\mathrm{F}} \tag{17}$$

For raffinate nodes,

$$Q_{\mathrm{IV}} = Q_{\mathrm{III}} - Q_{\mathrm{R}} \tag{18}$$

$$c_{i,k+1,\mathrm{in}} = c_{i,k}\big|_{t,z=L_{\mathrm{C}}} \tag{19}$$

$$c_{i,\mathrm{R}} = c_{i,k}\big|_{t,z=L_{\mathrm{C}}} \tag{20}$$

When two streams enter and exit between the two columns, the following occurs.

The eluent port and extract port gather at the same node when Zone I contains no column. The mass balance of this node can not be obtained simply by combining Equations (11)–(15) because of the special design of the node, which will be introduced in Section 3.1 of this article.

$$c_{i,k+1,\mathrm{in}} = \frac{Q_{\mathrm{IV}} - Q_{\mathrm{I}} + Q_{\mathrm{II}}}{Q_{\mathrm{II}}} c_{i,k}\big|_{t,z=L_{\mathrm{C}}} \tag{21}$$

$$c_{i,\mathrm{X}} = c_{i,k}\big|_{t,z=L_{\mathrm{C}}} \tag{22}$$

When Zone IV contains no column, the raffinate port and eluent port gather at the same node.

$$c_{i,k+1,\mathrm{in}} = \frac{Q_{\mathrm{IV}}}{Q_{\mathrm{I}}} c_{i,k}\big|_{t,z=L_{\mathrm{C}}} \tag{23}$$

$$c_{i,\mathrm{R}} = c_{i,k}\big|_{t,z=L_{\mathrm{C}}} \tag{24}$$

where Q_{D}, Q_{X}, Q_{F} and Q_{R} are the flow rates of desorbent, extract, feed and raffinate, respectively. $c_{i,\mathrm{X}}$ and $c_{i,\mathrm{R}}$ are the concentrations in the extract and raffinate stream, respectively.

2.2. Numerical Solving of the Model Equations

The mathematical model describing the dynamics of the VARICOL process consists of partial differential equations and nonlinear algebraic equations. gPROMS software with version 4.0.0, developed by Process System Enterprise, was applied to numerically solve the equations. The axial domains of all columns were discretized by orthogonal collocation on finite elements method (OCFEM) with third order over uniform grids. In our preliminary works, different interval numbers ranging from 10 to 100 were used for numerical solvation, and the effect of interval number on prediction accuracy and CPU time was studied. An interval number of 60 for discretization was selected, since it can minimize the computation efforts while ensuring the prediction accuracy of internal concentration profiles. The absolute and relative tolerance were set as 10^{-5}.

2.3. VARICOL Separation Performance Parameters

Parameters, including purity, productivity and solvent consumption, were defined for performance evaluation.

The purity of the extract is defined as the mass percentage of the more-adsorbed species in both enantiomers contained in the extract stream over a cycle during cyclic steady state. The purity of the raffinate is defined as the mass percentage of the less-adsorbed species in both enantiomers contained in the raffinate stream over a cycle during cyclic steady state.

$$PUR = \frac{\overline{c_{1,\mathrm{R}}}}{\sum_{i=1}^{2} \overline{c_{i,\mathrm{R}}}} \tag{25}$$

$$PUX = \frac{\overline{c_{2,\mathrm{X}}}}{\sum_{i=1}^{2} \overline{c_{i,\mathrm{X}}}} \tag{26}$$

The productivity is defined as the amount of racemate resolved by the VARICOL process per volume of chiral stationary phase per unit of time.

$$PR = \frac{Q_{\mathrm{F}} \sum_{i=1}^{2} c_{i,\mathrm{F}}}{(1-\varepsilon) N_{\mathrm{C}} V_{\mathrm{C}}} \tag{27}$$

where V_{C} is the volume of the column.

The solvent consumption is defined as the total volume of solvent used in both inlet streams per amount of racemate resolved by the VARICOL process.

$$SC = \frac{Q_{\mathrm{D}} + Q_{\mathrm{F}}}{Q_{\mathrm{F}} \sum_{i=1}^{2} c_{i,\mathrm{F}}} \tag{28}$$

2.4. Design of the VARICOL Process

To obtain relatively optimized separation performance, flow rates in each zone and shifting scheme, including initial column configurations and individual shifting time for all ports, should be suitably designed. In the VARICOL process, the shifting of an inlet or outlet port can be either upstream or downstream. If an inlet or outlet line is shifted upstream for one column, a downstream shifting for two columns is required for it in the period to ensure that the initial position of this line in the next period is a column downstream. Therefore, the simplest shifting schemes contain only a downstream movement of one column for all ports. It has been found that, among the possible shifting schemes with the same average column configurations, the simplest shifting scheme presents the best separation performance [55]. Though more than one simplest shifting scheme corresponds to a specific average column configuration, they are actually equivalent because they give the same product purities [55,56]. Thus, only the VARICOL process with the simplest shifting scheme is studied in this work, and the average column numbers in each zone can be used as decision variables for shifting scheme operation [56,57]. In this research, only symmetric average column configurations are considered. In other words, the average column number of Zone I and Zone IV is set to the same value, and the average column number of Zone II and Zone III is set to the same value as well in the VARICOL process.

Flow rate ratio m_j is a dimensionless parameter [58], defined as

$$m_j = \frac{Q_j^{\mathrm{TMB}}}{Q_{\mathrm{s}}} \tag{29}$$

The relationship between the SMB process and the corresponding TMB process is shown in the following:

$$Q_j = Q_j^{\mathrm{TMB}} + \frac{\varepsilon}{1-\varepsilon} Q_{\mathrm{s}} \tag{30}$$

$$Q_{\mathrm{s}} = \frac{(1-\varepsilon)V_{\mathrm{C}}}{t_{\mathrm{s}}} \tag{31}$$

where Q_j^{TMB} and Q_{s} are the flow rates of fluid and adsorbent particles in the corresponding TMB process, respectively. t_{s} is the period time of the SMB process.

To ensure the complete regeneration of the chiral stationary phase in Zone I and the eluent in Zone IV, the values of m_{I} and m_{IV} were chosen by

$$m_{\mathrm{I}} = \beta(H_2 + Q_{\max} b_2) \tag{32}$$

$$m_{\mathrm{IV}} = \frac{H_1 + Q_{\max} b_1}{\beta} \tag{33}$$

where H_1, H_2, $Q_{\max}$, b_1, and b_2 are the adsorption isotherm parameters in the modified linear + Langmuir model, and β is the safety margin. Herein, the value of β is set at 1.25 to fix the flow rate of Zone I and Zone IV, and thereby, the eluent flow rate is fixed [48,59]. From the definition of productivity and solvent consumption shown in Equations (27) and (28), in an SMB unit with fixed column numbers, with a higher flow rate of the feed stream, the productivity rises and solvent consumption drops. The multi-objective optimization containing productivity and solvent consumption as objective functions can thus be transformed to a single-objective optimization for maximizing the feed flow rate of the VARICOL unit. In our future research for optimizing the operation conditions of the VARICOL process, the effect of the value for m_{I} and m_{IV} on the productivity and solvent consumption should be further investigated.

The parameters related to adsorption equilibrium and kinetics at 25 °C were measured in our previous work [47], as listed in Table 1. Structure and operation designs are summarized in Table 2. The switching period and feed concentrations were set according to our previous work [47]. The purity requirement of both extract and raffinate was set at 95.0%. Separation regions for different average column configurations were obtained after simulating the VARICOL process with different pairs of ($m_{\mathrm{II}} \times m_{\mathrm{III}}$).

Table 1. Parameters related to adsorption equilibrium and kinetics.

Parameters		Value
Adsorption isotherm	H_1	0.504
	H_2	0
	$Q_{\max}$ (g/L)	265.94
	b_1 (L/g)	3.83×10^{-3}
	b_2 (L/g)	7.35×10^{-3}
Mass transfer coefficient	K (cm/s)	1.3×10^{-4}

Table 2. Design conditions for device structure and operation.

Design Conditions		Value
Structure parameter	L_{C} (cm)	15
	d_{C} (cm)	1
	d_{p} (cm)	2×10^{-3}
	ε	0.40
	Pe	3.4×10^{3}

Table 2. *Cont.*

Design Conditions		Value
Operation parameter	T (°C)	25
	$c_{1,F}$ (g/L)	10
	$c_{2,F}$ (g/L)	10
	t_s (min)	2
	m_I	2.44
	m_{IV}	1.22
	PUX	≥0.95
	PUR	≥0.95

2.5. Definitions of the Ports Shifting

To better describe the shifting of the four inlet and outlet ports in a simplest shifting scheme, a series of parameters is defined [55,56,60].

The shifting time of the ports can be normalized by the switching period,

$$\delta t_l = \frac{t_l}{t_s} \tag{34}$$

where l (l = D, X, F, R) refers to the inlet and outlet lines, with D, X, F, and R representing the desorbent, extract, feed, and raffinate, respectively. t_l is the switching time of the ports within a period, and δt_l is the normalized switching time.

Constraints of the normalized switching time are as follows:

$$0 < \delta t_l \leq 1 \tag{35}$$

It should be noted that at least one of the four normalized switching times must be 1, which symbolizes the finish of the period. When all the normalized switching times of the inlet and outlet lines are 1, the process becomes a conventional SMB process. Therefore, the conventional SMB process can be regarded as a special case of the VARICOL process.

The differences in the normalized switching time for two neighboring lines are given as

$$\delta x = \delta t_X - \delta t_D \tag{36}$$

$$\delta y = \delta t_F - \delta t_X \tag{37}$$

$$\delta z = \delta t_R - \delta t_F \tag{38}$$

With these definitions, the difference between the normalized switching time of any two ports can be described:

$$\delta t_F - \delta t_D = \delta x x + \delta y \tag{39}$$

$$\delta t_R - \delta t_X = \delta y + \delta z \tag{40}$$

$$\delta t_R - \delta t_D = \delta x + \delta y + \delta z \tag{41}$$

The constraints for these parameters can be inferred from Inequality (35):

$$-1 < \delta x < 1 \tag{42}$$

$$-1 < \delta y < 1 \tag{43}$$

$$-1 < \delta z < 1 \tag{44}$$

$$-1 < \delta x + \delta y < 1 \tag{45}$$

$$-1 < \delta y + \delta z < 1 \tag{46}$$

$$-1 < \delta x + \delta y + \delta z < 1 \tag{47}$$

The relationship between the initial column configuration and the average column configuration can be given by

$$\overline{N_I} = N_I^0 - \delta x \tag{48}$$

$$\overline{N_{II}} = N_{II}^0 - \delta y \tag{49}$$

$$\overline{N_{III}} = N_{III}^0 - \delta z \tag{50}$$

$$\overline{N_{IV}} = N_{IV}^0 + \delta x + \delta y + \delta z \tag{51}$$

where $\overline{N_j}$ is the average column number over a period, and N_j^0 is the initial column number at the beginning of a period.

In both the initial column configuration and average column configuration, the sum of the column numbers in all zones should be the total column numbers.

$$\sum_{j=I}^{IV} N_j^0 = N_C \tag{52}$$

$$\sum_{j=I}^{IV} \overline{N_j} = N_C \tag{53}$$

2.6. Derivation of the Shifting Scheme

To simulate or operate a VARICOL unit, the shifting scheme, including the initial column numbers in each zone and the shifting time for each port, should be derived from the average column configurations.

From Equations (48)–(51) and Inequalities (42)–(44) and (47), it can be inferred that, for the zones possessing integer average column numbers, their initial column numbers at the beginning of a period must be equal to their average column number. Moreover, for the zones that have rational average column numbers, which are fraction numbers, their initial column numbers are the nearest lower integer or nearest upper integer of the average column numbers, $\lceil \overline{N_j} \rceil$ or $\lceil \overline{N_j} \rceil + 1$, respectively. Meanwhile, the constraints for the initial column numbers in all zones, shown as Equation (52), must be fulfilled when the total column number is fixed. Thus, among the N_Z zones with rational average column numbers, the initial column numbers in $N_Z - N_C + \sum_{j=I}^{IV} \lceil \overline{N_j} \rceil$ zones should be assigned as $\lceil \overline{N_j} \rceil$, and the initial column numbers in $N_C - \sum_{j=I}^{IV} \lceil \overline{N_j} \rceil$ zones should be assigned as $\lceil \overline{N_j} \rceil + 1$. This leads to an option number for the nearest integer combinations of

$$N_{CC} = C_{N_Z}^{N_C - \sum_{j=I}^{IV} \lceil \overline{N_j} \rceil} \tag{54}$$

The option quantity of the nearest integer combinations for different zone numbers with rational average column numbers and the difference between the total column number and the sum of the nearest lower integer of the average column numbers are summarized in Table 3.

However, among these nearest integer combinations, some may not make physical sense when used as an initial column configuration, because they may not fulfill the Inequalities (45) and (46).

Table 3. Option number of the nearest integer combinations for different cases.

N_Z	4-N_Z	$N_C - \sum_{j=I}^{IV} [\overline{N_j}]$	N_{CC}
4	0	1	4
4	0	2	6
4	0	3	4
3	1	1	3
3	1	2	3
2	2	1	2

For all the obtained nearest integer combinations, the difference of the normalized switching time for two neighboring lines, δx, δy and δz, can be determined by Equations (48)–(50). The value of δx + δy and δy + δz can be further calculated, and the integer combinations that do not fulfill Inequalities (45) and (46) can be excluded.

For all the remaining possible initial column configuration options, the switching time of the four inlet and outlet lines giving the desired average column configuration should also be determined.

As explained before, the maximum value of the normalized switching time for the four ports must be 1. From Equations (36), (39) and (41), the normalized switching time of the eluent port can be determined by

$$\delta t_D = 1 - max\{0, \delta x, \delta x + \delta y, \delta x + \delta y + \delta z\} \quad (55)$$

The normalized switching time for other inlet and outlet ports can be determined by Equations (36)–(38) [56].

3. Experiments

3.1. Materials and Equipment

Racemic menthol, GC grade with a purity above 98%, was purchased from Tokyo Chemical Industry (Tokyo, Japan). n-hexane and 2-propanol, both HPLC grade with purities above 99.9%, were purchased from Fischer Scientific (Waltham, MA, USA). The preparative chiral stationary phase and analytical HPLC column Chiralpak AD-H (4.6 mm ID × 150 mm L) packed with analytical chiral stationary phase were purchased from Tokyo Daicel Chemical Industry (Tokyo, Japan). Both the preparative and analytical chiral stationary phases are amylose 3,5-dimethylphenylcarbamate coated on silica gel, commercially named Chiralpak AD, but they have different particle sizes of 20 μm and 5 μm, respectively. The preparative chiral stationary phase was packed in six stainless steel chromatographic columns (10 mm ID × 150 mm L) by the slurry method, which were used in the SMB separation. The hydrodynamic characteristics of these SMB columns, including bulk porosity and Peclet number, were measured in our previous study [47]. The relative errors of bulk porosity for these columns are less than 3.0%, showing good packing symmetry. The analytical column was used for the analysis of enantiomer concentrations.

VARICOL-micro is an SMB unit assembled by NOVASEP (Pompey, France). The device is equipped with five double piston pumps for the delivery of eluent, extract, feed, raffinate and recycling stream, respectively. An insulated chamber with air circulation and a heat exchanger is installed to control the operation temperature of the SMB columns, which can accommodate up to 8 columns. Another heat exchanger is installed to control the temperature of the two inlet streams, feed and eluent. The two heat exchangers are connected to a thermostatic bath. UV detector and polar detector are connected in the recycling line to online monitor the enantiomer concentrations. A six-port valve with a

250 μL loop is also installed in the recycling lines to facilitate the sample collections and obtain the internal concentration profiles. Two inlet lines and two outlet lines with individual valves are connected between every two neighboring columns for the purpose of VARICOL operation. The asynchronous port shifting can be realized by the opening and closing of these valves. Considering the case for temporarily superposition of two ports, the outlet lines are connected to the circulating lines in front of the inlet lines in the direction of the fluid flow [32], as shown in Figure 3. When Zone II or Zone III contains no column, the feed solution will not pollute the outlet product, and when Zone I or Zone IV contains no column, the eluent solution will not dilute the outlet product. The device configurations of the 6-column SMB unit and 5-column VARICOL unit are illustrated in Figure 4.

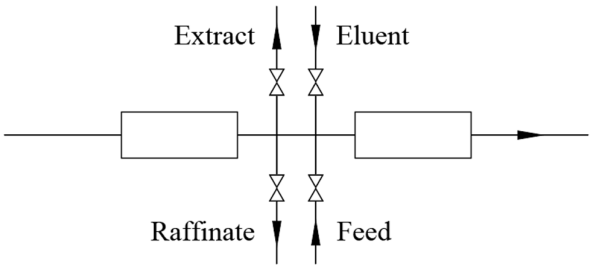

Figure 3. Connection of the inlet and outlet lines to the circulating lines.

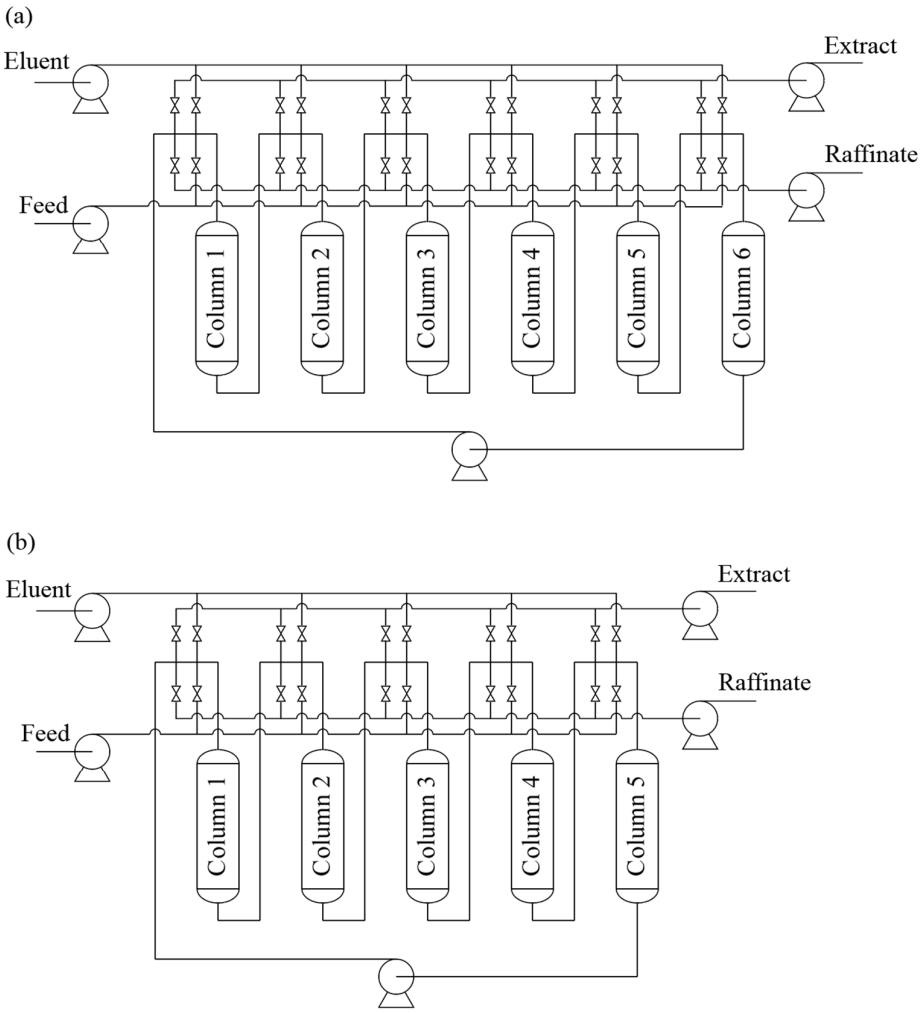

Figure 4. Schematic diagram of (**a**) 6-column SMB unit and (**b**) 5-column VARICOL unit configurations.

Ultimate 3000 is an analytical HPLC device purchased from Thermo Fischer Scientific (Waltham, MA, USA). It consists of a quaternary pump, autosampler, column oven and refractive index (RI) detector, and was used for the concentration determinations of menthol enantiomers.

3.2. SMB Operation

The eluent, n-hexane/2-propanol (95/5, v/v), was prepared by mixing 950 mL of n-hexane and 50 mL of 2-propanol, and the feed with a total concentration of 20 g/L was prepared by dissolving racemic menthol into the eluent. Both inlet solutions were filtered with 0.22 μm nylon filtration membranes and degassed in an ultrasonic bath after being freshly prepared. The flow rates of the five double piston pumps were corrected, and the SMB columns initially saturated with eluent were installed in the insulated chamber and then connected in series. The operation temperature was maintained by setting the temperature of the thermostatic bath. The designed operating conditions, including average column numbers in each zone, switching period and flow rates of eluent, feed, raffinate and recycling streams, were set on the control software (iFIX 4.5). The cyclic steady state was identified through the signals of the polar monitor. After reaching cyclic steady state, the outlet solution of extract and raffinate in an entire cycle was collected in order to evaluate the separation performance, and the solution at the recycling line was collected at 25%, 50%, 75% and 100% of each switching period using the six-port valve to obtain the internal concentration profiles.

It is worth noting that the recycling pump introduces an extra-column dead volume of 4 mL, as measured and recommended by the equipment producer. Two strategies were frequently used to design process conditions for SMB units with extra-column dead volume. The first strategy is applying an SMB model without considering extra-column dead volume, followed by operating the unit with compensation methods, while the second strategy includes the back-mixing occurred in the connecting lines into the mathematical model. It was found that the switching time compensation method, which belongs to the first strategy, and the second strategy predict almost overlapped separation regions for a micro-scale SMB unit [51]. The switching time compensation method was adopted in the present study because its mathematical model is simpler and requires less computational effort. The dead time caused by the recycling pump can be estimated by

$$t_{\mathrm{ED}} = \frac{V_{\mathrm{ED}}}{\overline{Q_j}} \tag{56}$$

where t_{ED} is the dead time caused by the extra-column dead volume. V_{ED} is the extra-column dead volume. $\overline{Q_j}$ is the average flow rate of each section in the SMB process. To compensate for the time delay, the dead time is added to the switching time of all the inlet and outlet ports passing through the last column and the recycling lines in the SMB process [32,48].

3.3. Assay

The concentrations of menthol enantiomers in samples were determined by the HPLC-RI method, which was adapted from the literature [61]. The Chiralpak AD-H analytical column was used, with n-hexane/2-propanol (99/1, v/v) as the mobile phase in order to achieve a higher resolution. The temperature of the column oven and refractive index detector were set at 25 °C and 35 °C, respectively. The flow rate of the mobile phase was 1 mL/min, and the sample injection volume was 10 μL. The retention times of d-menthol and l-menthol were 8.38 min and 9.91 min, respectively, and the resolution was 2.62. External standard calibration curves with a single enantiomer concentration range of

0.040 g/L–2 g/L were used for quantitative analysis. The calibration curves of d-menthol and l-menthol were Y = 1.2422X + 0.0107 and Y = 1.2215X + 0.0094, respectively, where Y represents the peak area with unit of μRIU·min, and X represents enantiomer concentration with unit of g/L.

4. Results and Discussion

4.1. VARICOL Process Optimization

The possible shifting schemes, including the initial column numbers in each zone and shifting time for each port in the six-column VARICOL process with average column configuration of $\theta/(3-\theta)/(3-\theta)/\theta$ ($0.5 < \theta < 1$), are listed in Table 4.

Table 4. Possible initial column configurations and individual switching times of the inlet and outlet ports for the 6-column VARICOL process with an average column configuration of $\theta/(3-\theta)/(3-\theta)/\theta$ ($0.5 < \theta < 1$).

Parameters	Option 1	Option 2	Option 3
${N_{\mathrm{I}}}^0$	0	1	1
${N_{\mathrm{II}}}^0$	3	2	2
${N_{\mathrm{III}}}^0$	2	2	3
${N_{\mathrm{IV}}}^0$	1	1	0
δt_{D}	1	θ	$1-\theta$
δt_{X}	$1-\theta$	1	$2-2\theta$
δt_{F}	1	θ	$1-\theta$
δt_{R}	θ	$2\theta-1$	1

A possible shifting scheme, option 1 in Table 4, was used for the simulation of separation performance, as illustrated in Figure S1 of the Supplementary Materials. The initial column configuration in a period is 0/3/2/1, where the eluent line and extract line meet at the same port, because Zone I has no column. The extract stream is withdrawn from the outlet stream of the column in Zone IV before the remaining stream mixes with the inlet eluent stream because of the special design of the ports. After $(1-\theta)t_{\mathrm{s}}$, the extract line shifts downstream for a column, and the column configuration changes to 1/2/2/1. After $(2\theta-1)t_{\mathrm{s}}$, the raffinate line shifts downstream for a column, and the column configuration changes to 1/2/3/0, where the raffinate line and eluent line meet at the same port, because Zone IV has no column. The raffinate stream is withdrawn from the outlet stream of the column in Zone III before the remaining stream mixes with the inlet eluent stream. After $(1-\theta)t_{\mathrm{s}}$, the eluent and feed lines shift downstream for a column simultaneously, and the column configuration changes to 0/3/2/1 for the next period.

The separation regions of VARICOL processes with average column configuration of $\theta/(3-\theta)/(3-\theta)/\theta$ ($0.5 < \theta < 1$) and conventional SMB with column configuration of 1/2/2/1 were estimated by simulations, as shown in Figure 5.

For each average column configuration, the vertex points in the separation regions possess the highest feed flow rate, and thereby the highest productivity and lowest solvent consumption, so it is recognized as the optimal operation point. The separation performance of the optimal operation points for 6-column VARICOL and conventional SMB processes with different average column configuration are compared, as listed in Table 5. At optimized operation conditions, the VARICOL process with average column configuration of 0.9/2.1/2.1/0.9 and 0.8/2.2/2.2/0.8 has a greater feed flow rate and productivity, less solvent consumption compared with the process of 1/2/2/1. This can be partly explained by the increased column number of Zone II and Zone III in the VARICOL process, which is mainly responsible for the separation of the enantiomers. However, as the value of θ further decreases from 0.8, the feed flow rate and productivity seem to show

a decreasing trend, and solvent consumption increases at the optimal point, which may be related to the poorer regeneration of the stationary phase and mobile phase with shorter average column length in Zone I and Zone IV.

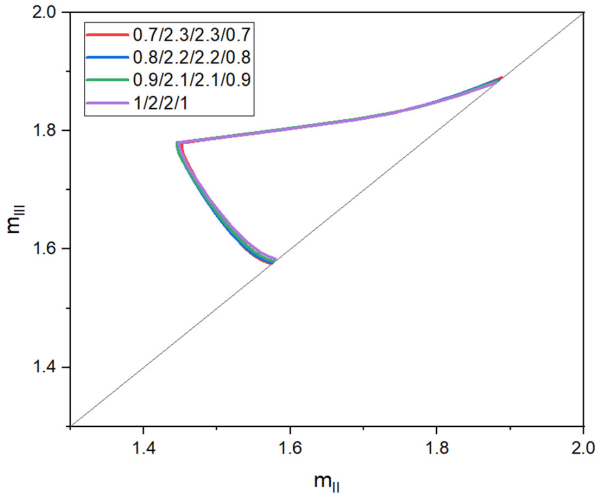

Figure 5. Comparison of the separation regions for 6-column conventional SMB and VARICOL processes with different average column configurations. Purity requirements, 95.0% for both extract and raffinate. Period time, 2 min. Flow rate ratios in Zone I and Zone IV, 2.44 and 1.22, respectively. Racemic menthol feed concentration, 20 g/L. Column configuration of conventional SMB, 1/2/2/1. Average column configuration of VARICOL, $\theta/(3-\theta)/(3-\theta)/\theta$, $0.5 < \theta < 1$.

Table 5. Separation performance of the optimal operation points for the 6-column VARICOL and conventional SMB process with different average column configurations. Purity requirements, 95.0% for both extract and raffinate. Period time, 2 min. Flow rate ratios in Zone I and Zone IV, 2.44 and 1.22, respectively. Racemic menthol feed concentration, 20 g/L.

Average Column Configurations	$Q_{F,max}$ (mL/min)	PR_{max} ($g_{racemate}/(L_{CSP}\cdot min)$)	SC_{min} ($L/g_{racemate}$)
0.7/2.3/2.3/0.7	1.159	0.547	0.236
0.8/2.2/2.2/0.8	1.184	0.558	0.232
0.9/2.1/2.1/0.9	1.184	0.558	0.232
1/2/2/1	1.177	0.555	0.233

The possible shifting scheme, including the initial column numbers in each zone and shifting time for each port in the five-column VARICOL process, with an average column configuration of $\theta/(2.5-\theta)/(2.5-\theta)/\theta$ ($0.5 < \theta < 1$) and 1/1.5/1.5/1, is listed in Tables 6 and 7, respectively.

Table 6. Possible initial column configurations and individual switching times of the inlet and outlet ports for a 5-column VARICOL process with an average column configuration of $\theta/(2.5-\theta)/(2.5-\theta)/\theta$ ($0.5 < \theta < 1$).

Parameters	Option 1	Option 2	Option 3	Option 4
N_I^0	0	1	1	1
N_{II}^0	2	1	2	2
N_{III}^0	2	2	1	2
N_{IV}^0	1	1	1	0
δt_D	1	θ	0.5	$1-\theta$
δt_X	$1-\theta$	1	$1.5-\theta$	$2-2\theta$
δt_F	0.5	$\theta-0.5$	1	$1.5-\theta$
δt_R	θ	$2\theta-1$	$\theta-0.5$	1

Table 7. Possible initial column configurations and individual switching times of the inlet and outlet ports for a 5-column VARICOL process with an average column configuration of 1/1.5/1.5/1.

Parameters	Option 1	Option 2
$N_I{}^0$	1	1
$N_{II}{}^0$	1	2
$N_{III}{}^0$	2	1
$N_{IV}{}^0$	1	1
δt_D	1	0.5
δt_X	1	0.5
δt_F	0.5	1
δt_R	1	0.5

Possible shifting schemes, Option 1 in Table 6 and Option 1 in Table 7, were used for the simulation of separation performance, as illustrated in Figure S2 and Figure S3 of the Supplementary Materials, respectively. The separation region of the VARICOL process with average column configuration of $\theta/(2.5-\theta)/(2.5-\theta)/\theta$ $(0.5 < \theta \leq 1)$ and conventional SMB with column configuration of 1/1/2/1 and 1/2/1/1 were estimated by simulations, as shown in Figure 6.

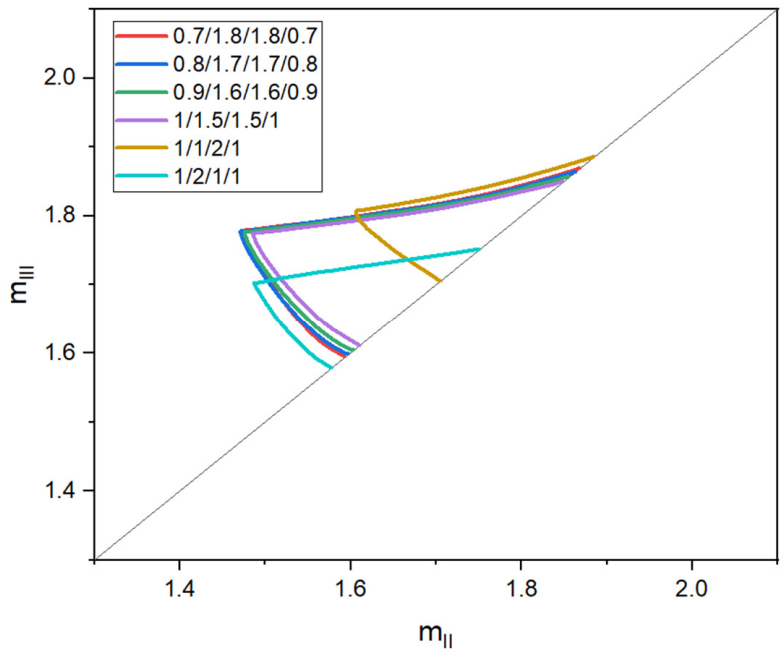

Figure 6. Comparison of the separation region for the 5-column conventional SMB and VARICOL process with different average column configurations. Purity requirements are 95.0% for both extract and raffinate. Period time, 2 min. Flow rate ratios in Zone I and Zone IV, 2.44 and 1.22, respectively. Racemic menthol feed concentration, 20 g/L. Column configuration of conventional SMB, 1/2/1/1 and 1/1/2/1. Average column configuration of VARICOL, $\theta/(2.5-\theta)/(2.5-\theta)/\theta$ $(0.5 < \theta \leq 1)$.

The separation performance of the optimal operation points for the five-column VARICOL and conventional SMB processes with different average column configuration are compared, as listed in Table 8. Similarly to the case with six columns, with a decreasing value of θ, a peak of feed flow rate, productivity and solvent consumption can also be found.

Figure 7 compares the feed flow rate, productivity and solvent consumption under the optimized operation point of both VARICOL and conventional SMB with optimal average column configurations for a total column number of five or six. For both cases with a fixed

total column number of five or six, the VARICOL process can achieve a greater feed flow rate, and thereby, higher productivity and lower solvent consumption than the conventional SMB process, indicating a lower operation cost of the VARICOL process. This verified the universal superiority of the VARICOL process against conventional SMB in terms of separation performance, regardless of the outlet purity setpoint, thanks to the additional degree of freedom in operation offered by the asynchronous shifting mode. Whereas the separation performance is slightly improved by using the VARICOL process in a six-column unit, the productivity of the VARICOL process is 42.2% higher than the conventional SMB process in a five-column unit. It seems that the superiority is more pronounced when the total column number is five, which may be related to the very limited choice of column configurations with low total column numbers. As can be seen in Figure 7, the productivity of the five-column conventional SMB process under optimized operation conditions is low in comparison with the six-column conventional SMB process. In contrast, the five-column VARICOL process presents a productivity higher than that of the six-column conventional SMB process under optimized operating conditions, reflecting that the superiority of the former process over the latter process is derived from the asynchronous switching manner instead of solely the reduction of column numbers. It is also worth noting that the five-column VARICOL unit with an average column configuration of 0.8/1.7/1.7/0.8 presents a comparable feed flow rate, and thereby, higher productivity and comparable solvent consumption with the six-column 1/2/2/1 conventional SMB. This implies the lower fixed cost, containing device and stationary phase cost in the VARICOL process with a column removed from the separation unit. Figure 8 illustrates the estimated separation region of 0.8/1.7/1.7/0.8 and 1/2/2/1 under a product purity target of 95.0%, demonstrating comparable operation regions.

Table 8. Separation performance of the optimal operation points for the 5-column conventional SMB and VARICOL process with different average column configurations. Purity requirements, 95.0% for both extract and raffinate. Period time, 2 min. Flow rate ratios in Zone I and Zone IV, 2.44 and 1.22, respectively. Racemic menthol feed concentration, 20 g/L.

Average Column Configurations	$Q_{F,max}$ (mL/min)	PR_{max} ($g_{racemate}/(L_{CSP} \cdot min)$)	SC_{min} ($L/g_{racemate}$)
0.7/1.8/1.8/0.7	1.074	0.608	0.251
0.8/1.7/1.7/0.8	1.085	0.614	0.249
0.9/1.6/1.6/0.9	1.064	0.602	0.253
1/1.5/1.5/1	1.025	0.58	0.260
1/2/1/1	0.763	0.432	0.332
1/1/2/1	0.710	0.402	0.353

It must be pointed out that a VARICOL unit with fewer total column numbers can be inferior to a conventional SMB unit in terms of separation performance under optimized operation conditions, particularly when the product purity target is high [56]. Figure 9 compares the simulated maximum productivity of the five-column 0.8/1.7/1.7/0.8 VARICOL unit and the six-column 1/2/2/1 conventional SMB unit under different outlet purity requirements. At an outlet purity requirement below approximately 98.0%, a 0.8/1.7/1.7/0.8 VARICOL unit can achieve productivity higher than a 1/2/2/1 conventional SMB unit. In contrast, conventional SMB with a 1/2/2/1 configuration is beneficial with a purity setpoint higher than 98.0%. This is because with a stringent outlet purity requirement, the separation efficiency dropped due to reduced column numbers, which is more prominent, and therefore can not be fully compensated for by optimizing the column number distribution.

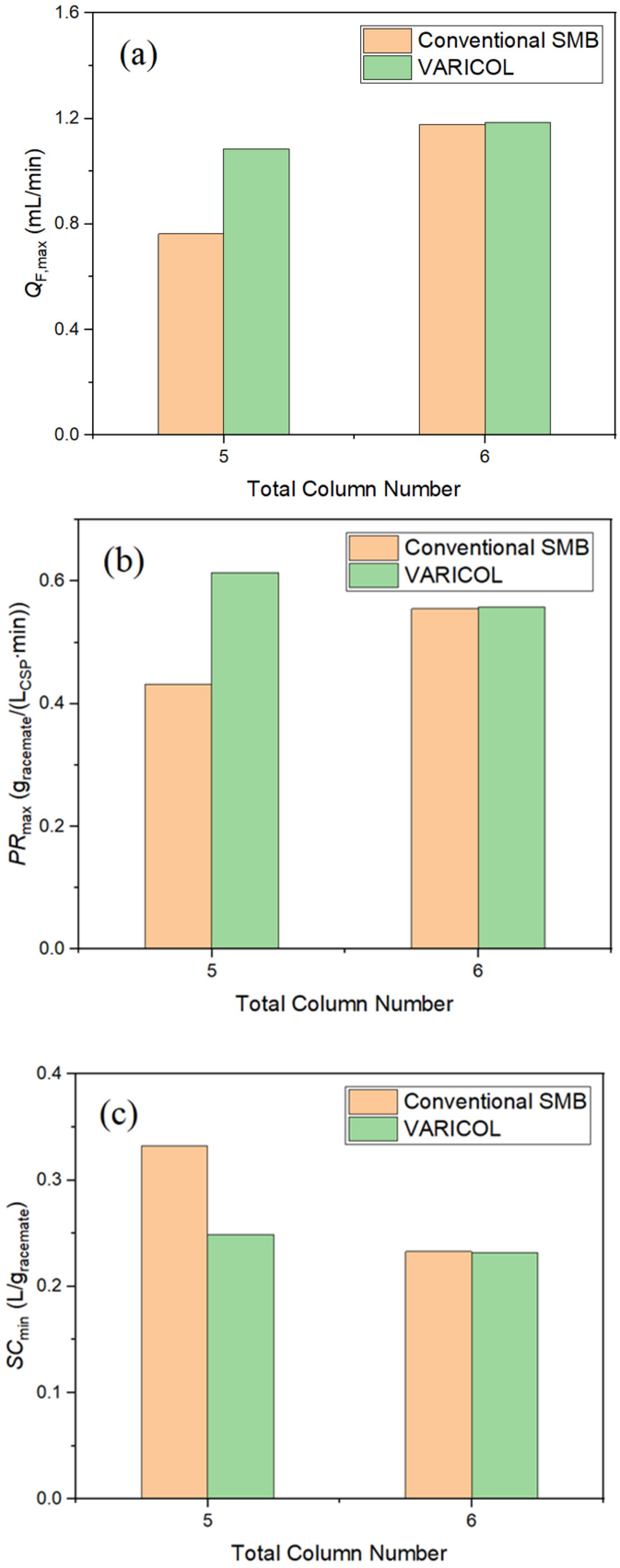

Figure 7. Comparison of (**a**) feed flow rate, (**b**) productivity, and (**c**) solvent consumption under optimized operation point for VARICOL and conventional SMB with optimal average column configurations. Purity requirements, 95.0% for both extract and raffinate. Period time, 2 min. Flow rate ratios in Zone I and Zone IV, 2.44 and 1.22, respectively. Racemic menthol feed concentration, 20 g/L.

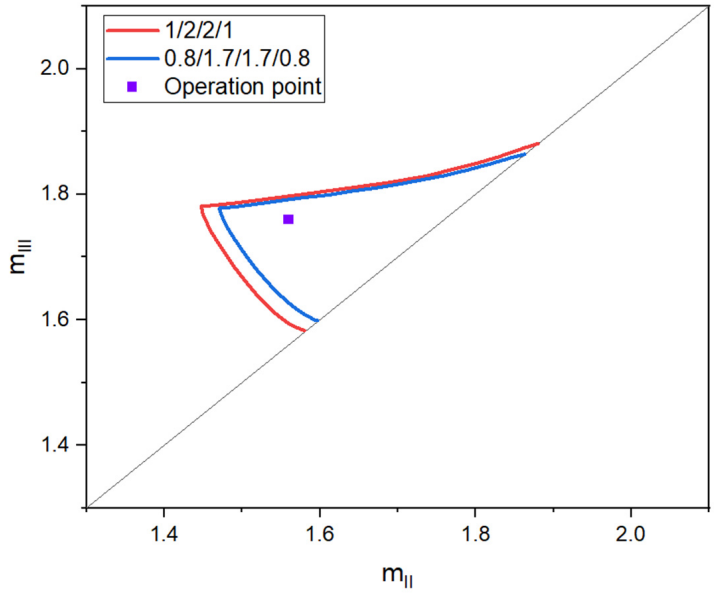

Figure 8. Separation region and operation point of 5-column 0.8/1.7/1.7/0.8 VARICOL and 6-column 1/2/2/1 conventional SMB process. Purity requirements, 95.0% for both extract and raffinate. Period time, 2 min. Flow rate ratios in Zone I and Zone IV, 2.44 and 1.22, respectively. Racemic menthol feed concentration, 20 g/L.

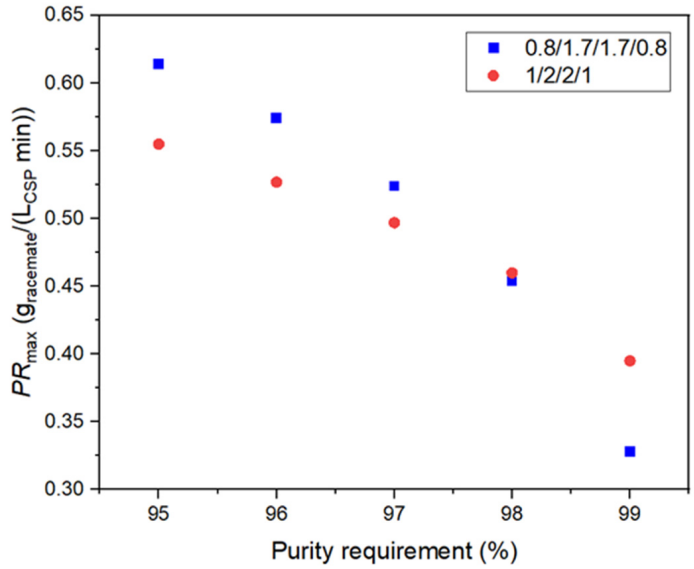

Figure 9. Effect of outlet purity requirement on maximum productivity of 5-column 0.8/1.7/1.7/0.8 VARICOL unit and 6-column 1/2/2/1 conventional SMB unit. Period time, 2 min. Flow rate ratios in Zone I and Zone IV, 2.44 and 1.22, respectively. Racemic menthol feed concentration, 20 g/L.

4.2. SMB Experiment

To demonstrate the superiority of the VARICOL process in terms of separation performance, a five-column VARICOL with an average column configuration of 0.8/1.7/1.7/0.8 and a six-column conventional SMB process with a column configuration of 1/2/2/1 were chosen for the resolution of menthol racemate under an outlet purity target of 95.0%, since they present the highest predicted productivity under optimized operation conditions among the VARICOL processes and conventional SMB process compared in the previous section, respectively. A pair of (m_{II} × m_{III}) was selected inside the separation region for both of the two processes in order to compare them more conveniently, as shown in Figure 8, and the corresponding operation conditions are listed in Table 9. For both

operation modes, a cyclic steady state was reached after operating 15 cycles. Samples were taken at the six-way valve located at the circulating line and subsequently analyzed to obtain the internal concentration profile at half of the switching period during cyclic steady state, which is compared with the predicted curve in Figure 10. Table 10 lists the experimental and simulated separation performances in cyclic steady state, and the analytic HPLC chromatograms of the outlet product in the VARICOL unit are displayed in Figure S4 of the Supplementary Materials. Good agreements can be found between the simulated results and the experimental results, though discrepancies may be derived from uncertainty in the estimation of model parameters, packing and tubing asymmetries, backmixing in connecting lines, and flow rate fluctuations in recycling and external streams. In both conventional SMB and VARICOL processes, purities of both outlet products were above 95.0%, and solvent consumptions of 0.355 L/$g_{racemate}$ were achieved. The productivity of the VARICOL process was 0.400 $g_{racemate}/(L_{CSP}\cdot min)$, which was 20% higher than the conventional SMB process because of the reduced columns, despite the 1.6% and 1.8% lower purities for raffinate and extract in the VARICOL process, respectively. The sensitivity of the isotherm parameter H_i on internal concentration profiles is also analyzed, as shown in Figure 11. $0.9H_i$ shows a slightly higher product purity, while $1.1H_i$ presents lower predicted purities in both outlet streams, reflecting the importance of estimation accuracy for VARICOL unit design.

Table 9. Operation conditions of VARICOL and conventional SMB process [47].

Operation Conditions	Conventional SMB	VARICOL
Temperature (°C)	25	
Total feed concentration (g/L)	20	
Average column configuration	1/2/2/1	0.8/1.7/1.7/0.8
Packing amount of chiral stationary phase (mL)	42.41	35.34
t_s (min)	2	
Q_F (mL/min)	0.71	
Q_X (mL/min)	3.11	
Q_R (mL/min)	1.91	
Q_D (mL/min)	4.31	
Q_I (mL/min)	10.98	
Q_{II} (mL/min)	7.87	
Q_{III} (mL/min)	8.58	
Q_{IV} (mL/min)	6.67	

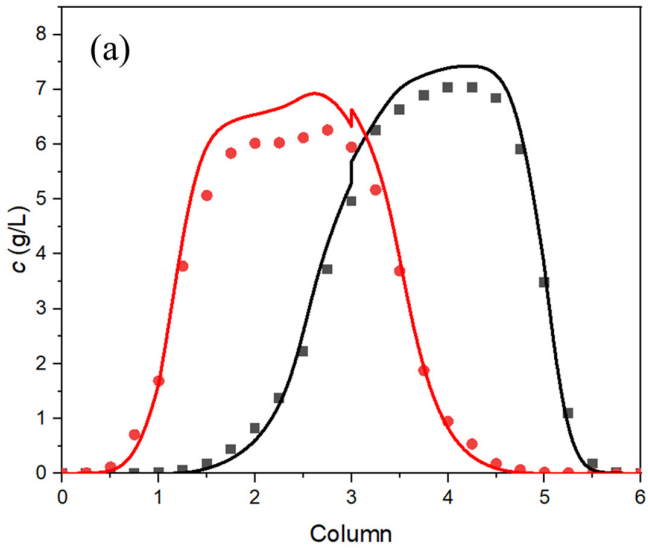

Figure 10. *Cont.*

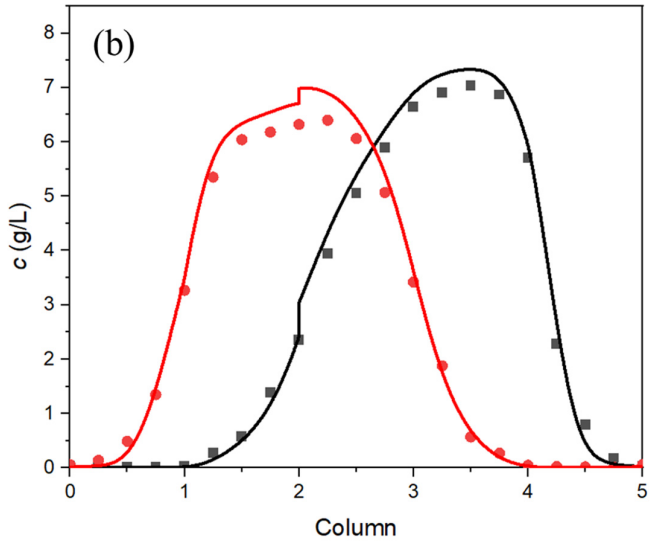

Figure 10. Experimental and predicted internal concentration profiles at the middle of the switching period during the cyclic steady state of (**a**) conventional SMB; (**b**) VARICOL process. Lines: predicted curves; points: experimental data. Black lines and points for d-menthol, and red lines and points for l-menthol.

Table 10. Experimental and simulated separation performance of VARICOL and conventional SMB process.

Separation Performance		Conventional SMB	VARICOL
$\overline{c_{1,R}}$ (g/L)	Experimental	3.62	3.56
	Simulated	3.69	3.66
$\overline{c_{2,R}}$ (g/L)	Experimental	0.0739	0.133
	Simulated	0.0156	0.0472
$\overline{c_{1,X}}$ (g/L)	Experimental	0.0574	0.0989
	Simulated	0.0123	0.0338
$\overline{c_{2,X}}$ (g/L)	Experimental	2.24	2.20
	Simulated	2.24	2.22
PUR (%)	Experimental	98.0	96.4
	Simulated	99.6	98.7
PUX (%)	Experimental	97.5	95.7
	Simulated	99.5	98.5
PR ($g_{racemate}/(L_{CSP}\cdot min)$)		0.333	0.400
SC ($L/g_{racemate}$)		0.355	0.355

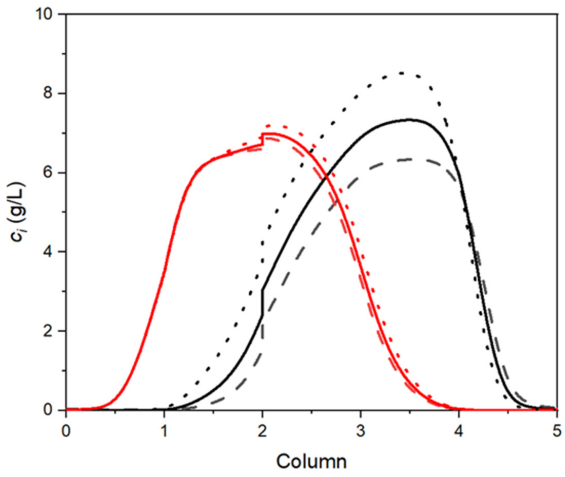

Figure 11. Simulated internal concentration profiles at the middle of the switching period during the cyclic steady state of the VARICOL process with different isotherm parameters of H_i. Solid lines: H_i; dashed lines: $0.9H_i$; dotted lines: $1.1H_i$. Black lines for d-menthol, and red lines for l-menthol.

5. Conclusions

This work intends to develop the chiral separation process of racemic menthol on Chiralpak AD chiral stationary phase by the VARICOL process to enhance the productivity. A mathematical model was developed for the design and optimization of the VARICOL process. Prediction results show that, when the total column number is five or six, asynchronous shifting of the inlet and outlet ports can provide higher productivity and lower solvent consumption than the conventional SMB process. Moreover, the five-column VARICOL process is found to possess a comparable separation region, and thereby, comparable feed and eluent flow rates with the six-column conventional SMB process under a product purity setpoint of 95.0%. 0.8/1.7/1.7/0.8 VARICOL process and 1/2/2/1 conventional SMB process with the same switching period and flow rate in all zones were carried out for the resolution of racemic menthol. In the VARICOL process, purities for both the extract and raffinate were above 95.0%, and a productivity of 0.400 $g_{racemate}/(L_{CSP} \cdot min)$ and a solvent consumption of 0.355 $L/g_{racemate}$ were achieved. The productivity was 20% higher than the conventional SMB process with the same solvent consumption at the price of slightly decreased product purities.

Supplementary Materials: The following supporting information can be downloaded at: https://www.mdpi.com/article/10.3390/separations13030095/s1, Figure S1: Evolution of the inlet and outlet ports positions over a period for the VARICOL process with 6 columns and an average column configuration of $\theta/(3-\theta)/(3-\theta)/\theta$ $(0.5 < \theta < 1)$; Figure S2: Evolution of the inlet and outlet ports positions over a period for the VARICOL process with 5 columns and an average column configuration of $\theta/(2.5-\theta)/(2.5-\theta)/\theta$ $(0.5 < \theta < 1)$; Figure S3: Evolution of the inlet and outlet ports positions over a period for the VARICOL process with 5 columns and an average column configuration of 1/1.5/1.5/1; Figure S4: Analytical HPLC chromatogram of (a) raffinate and (b) extract stream in VARICOL experiment.

Author Contributions: Conceptualization: L.S. and J.Y.; Methodology, L.S.; Software, L.S.; Validation, L.S. and Y.Y.; Formal Analysis, L.S.; Investigation, L.S.; Resources, Y.Y. and J.Y.; Data Curation, L.S.; Writing—Original Draft Preparation, L.S.; Writing—Review & Editing, Y.Y. and J.Y.; Visualization, L.S.; Supervision, Y.Y. and J.Y.; Project Administration, J.Y.; Funding Acquisition, J.Y. All authors have read and agreed to the published version of the manuscript.

Funding: This work was supported by the National Key R&D Program of China [grant number 2023YFB4104000]. This work was also supported by the Key Research and Development Program of Jiang-xi Province [20223BBG74008] and the ECUST-Jinghao Salt Chemical Carbon and Calcium Cycles Joint Research Centre.

Data Availability Statement: The original contributions presented in this study are included in the article/Supplementary Materials. Further inquiries can be directed to the corresponding authors.

Conflicts of Interest: The authors declare no conflicts of interest.

Nomenclature

b	Langmuir parameter (L/g)
c	Liquid phase concentration (g/L)
d_C	Column diameter (cm)
d_p	Particle diameter of the chiral stationary phase (μm)
D_{ax}	Axial dispersion coefficient (cm^2/s)
H	Henry constant (dimensionless)
K	Overall mass transfer coefficient (cm/s)
L_C	Column length (cm)

m	Flow rate ratio of the liquid phase and solid phase in the TMB process (dimensionless)
N	Column number in each zone (dimensionless)
N^0	Initial column number in each zone at the beginning of a period (dimensionless)
N_C	Total column number (dimensionless)
N_{CC}	Option number of the combinations for the nearest integer of the average column number in each zone (dimensionless)
N_Z	Zone number with rational average column numbers (dimensionless)
Pe	Peclet number (dimensionless)
PR	Productivity ($g_{racemate}/(L_{CSP}\cdot min)$)
PUR	Purity in raffinate stream (dimensionless)
PUX	Purity in extract stream (dimensionless)
q	Solid phase concentration (g/L)
q^*	Solid phase concentration equilibrium with the liquid phase concentration (g/L)
Q	Liquid flow rate in SMB columns (mL/min)
Q_{max}	Langmuir parameter (g/L)
Q_s	Solid phase flow rate in TMB process (mL/min)
Q^{TMB}	Liquid phase flow rate in TMB process (mL/min)
SC	Solvent consumption ($L/g_{racemate}$)
t	Time (min)
t_{ED}	Extra-column dead time (min)
t_s	Period time in VARICOL process (min)
u	Superficial velocity (cm/s)
V_C	Column volume (mL)
V_{ED}	Extra-column dead volume (mL)
z	Axial position (cm)
Subscripts	
D	Eluent stream
F	Feed stream
i	Component in the racemate (i = 1, 2)
in	Inlet position
j	Zone number (j = I, II, III, IV)
k	Column number (k = 1, 2, . . ., N_C)
l	External lines (l = D, X, F, R)
R	Raffinate stream
X	Extract stream
Greek symbols	
β	Safety factor (dimensionless)
δt	Normalized switching time for individual external ports (dimensionless)
δx	The difference of the normalized switching time for extract and eluent ports (dimensionless)
δy	The difference of the normalized switching time for feed and extract ports (dimensionless)
δz	The difference of the normalized switching time for raffinate and feed ports (dimensionless)
ε	Bed porosity (dimensionless)
θ	The average column number in Zone I and Zone IV (dimensionless)

References

1. Hughes, P. Flavors (Bittering Agents, Astringent Flavors, Pungency, Menthol). In *Encyclopedia of Food Chemistry*; Melton, L., Shahidi, F., Varelis, P., Eds.; Elsevier: Amsterdam, The Netherlands, 2019; Volume 1, pp. 104–108, ISBN 978-0-12-814045-1.
2. Kamatou, G.P.P.; Vermaak, I.; Viljoen, A.M.; Lawrence, B.M. Menthol: A Simple Monoterpene with Remarkable Biological Properties. *Phytochemistry* **2013**, *96*, 15–25. [CrossRef]
3. Dylong, D.; Hausoul, P.J.C.; Palkovits, R.; Eisenacher, M. Synthesis of (−)-menthol: Industrial Synthesis Routes and Recent Development. *Flavour Frag. J.* **2022**, *37*, 195–209. [CrossRef]
4. Schaefer, B. Flavours and Fragrances. In *Natural Products in the Chemical Industry*; Schaefer, B., Ed.; Springer: Berlin, Germany, 2014; pp. 45–168, ISBN 978-3-642-54461-3.
5. Asakawa, Y. Dietary Monoterpenoids. In *Handbook of Dietary Phytochemicals*; Xiao, J., Sarker, S.D., Asakawa, Y., Eds.; Springer: Singapore, 2021; pp. 1–124, ISBN 9789811317453.
6. Su, X.; Po, A.L.W.; Millership, J.S. Ciliotoxicity of Intranasal Formulations: Menthol Enantiomers. *Chirality* **1993**, *5*, 58–60. [CrossRef]
7. Murthy, P.B.K.; Ahmed, M.M.; Regu, K. Lack of genotoxicity of menthol in chromosome aberration and sister chromatid exchange assays using human lymphocytes in vitro. *Toxicol. Vitro* **1991**, *5*, 337–340. [CrossRef] [PubMed]
8. Kuhn, W.; Funk, H.-U.; Senft, G.; Korber, K.A. Method for Producing Menthol. U.S. Patent US2006167322A1, 27 July 2006.
9. Fleischer, J.; Bauer, K.; Hopp, R. Separating Optically Pure d- and l-Isomers of Menthol, Neomenthol and Isomenthol. U.S. Patent US3943181A, 9 March 1976.
10. Bai, S.; Guo, Z.; Liu, W.; Sun, Y. Resolution of (±)-Menthol by Immobilized Candida Rugosa Lipase on Superparamagnetic Nanoparticles. *Food Chem.* **2006**, *96*, 1–7. [CrossRef]
11. Ren, M.; Bai, S.; Zhang, D.; Sun, Y. pH Memory of Immobilized Lipase for (±)-Menthol Resolution in Ionic Liquid. *J. Agric. Food Chem.* **2008**, *56*, 2388–2391. [CrossRef]
12. Dudas, J.; Hanika, J. Design, Scale up and Safe Piloting of Thymol Hydrogenation and Menthol Racemisation. *Chem. Eng. Res. Des.* **2009**, *87*, 83–90. [CrossRef]
13. Wang, D.; Nag, A.; Lee, G.; Shaw, J. Factors Affecting the Resolution of *Dl* -Menthol by Immobilized Lipase-Catalyzed Esterification in Organic Solvent. *J. Agric. Food Chem.* **2002**, *50*, 262–265. [CrossRef]
14. Brady, D.; Reddy, S.; Mboniswa, B.; Steenkamp, L.H.; Rousseau, A.L.; Parkinson, C.J.; Chaplin, J.; Mitra, R.K.; Moutlana, T.; Marais, S.F.; et al. Biocatalytic Enantiomeric Resolution of L-Menthol from an Eight Isomeric Menthol Mixture through Transesterification. *J. Mol. Catal. B-Enzym.* **2012**, *75*, 1–10. [CrossRef]
15. Toribio, L.; Magdaleno, I.; Martín-Gómez, B.; Martín, M.T.; Valverde, S.; Ares, A.M. Study of Different Chiral Columns for the Enantiomeric Separation of Azoles Using Supercritical Fluid Chromatography. *Separations* **2022**, *10*, 9. [CrossRef]
16. Wojda, E.; Urbańska, M. The Application of Polysaccharide Chiral Columns for the Separation of Fluorinated and Protonated Liquid Crystalline Racemic Esters. *Separations* **2024**, *11*, 214. [CrossRef]
17. Jurin, M.; Kontrec, D.; Roje, M. HPLC and SFC Enantioseparation of (±)-Trans-β-Lactam Ureas on Immobilized Polysaccharide-Based Chiral Stationary Phases—The Introduction of Dimethyl Carbonate as an Organic Modifier in SFC. *Separations* **2024**, *11*, 38. [CrossRef]
18. Jurin, M.; Kontrec, D.; Dražić, T.; Roje, M. Enantioseparation of Syn- and Anti-3,5-Disubstituted Hydantoins by HPLC and SFC on Immobilized Polysaccharides-Based Chiral Stationary Phases. *Separations* **2022**, *9*, 157. [CrossRef]
19. Bolognino, I.; Carrieri, A.; Purgatorio, R.; Catto, M.; Caliandro, R.; Carrozzini, B.; Belviso, B.D.; Majellaro, M.; Sotelo, E.; Cellamare, S.; et al. Enantiomeric Separation and Molecular Modelling of Bioactive 4-Aryl-3,4-Dihydropyrimidin-2(1H)-One Ester Derivatives on Teicoplanin-Based Chiral Stationary Phase. *Separations* **2021**, *9*, 7. [CrossRef]
20. Sá Gomes, P.; Rodrigues, A.E. Simulated Moving Bed Chromatography: From Concept to Proof-of-Concept. *Chem. Eng. Technol.* **2012**, *35*, 17–34. [CrossRef]
21. Kniep, H.; Mann, G.; Vogel, C.; Seidel-Morgenstern, A. Separation of Enantiomers through Simulated Moving-Bed Chromatography. *Chem. Eng. Technol.* **2000**, *23*, 853–857. [CrossRef]
22. Azevedo, D.C.S.; Rodrigues, A.E. Fructose–Glucose Separation in a SMB Pilot Unit: Modeling, Simulation, Design, and Operation. *AICHE J.* **2001**, *47*, 2042–2051. [CrossRef]
23. Subramani, H.J.; Hidajat, K.; Ray, A.K. Optimization of Simulated Moving Bed and Varicol Processes for Glucose–Fructose Separation. *Chem. Eng. Res. Des.* **2003**, *81*, 549–567. [CrossRef]
24. Arafah, R.S.; Ribeiro, A.E.; Rodrigues, A.E.; Pais, L.S. Separation of Nadolol Racemates by High pH Reversed-Phase Fixed-Bed and Simulated Moving Bed Chromatography. *Sep. Purif. Technol.* **2023**, *305*, 122529. [CrossRef]
25. Pais, L.S.; Loureiro, J.M.; Rodrigues, A.E. Separation of Enantiomers of a Chiral Epoxide by Simulated Moving Bed Chromatography. *J. Chromatogr. A* **1998**, *827*, 215–233. [CrossRef]
26. Ribeiro, A.E.; Gomes, P.S.; Pais, L.S.; Rodrigues, A.E. Chiral Separation of Ketoprofen Enantiomers by Preparative and Simulated Moving Bed Chromatography. *Sep. Sci. Technol.* **2011**, *46*, 1726–1739. [CrossRef]

27. Vaňková, K.; Polakovič, M. Design of Fructooligosaccharide Separation Using Simulated Moving-Bed Chromatography. *Chem. Eng. Technol* **2012**, *35*, 161–168. [CrossRef]
28. Paredes, G.; Makart, S.; Stadler, J.; Mazzotti, M. Simulated Moving Bed Operation for Size Exclusion Plasmid Purification. *Chem. Eng. Technol* **2005**, *28*, 1335–1345. [CrossRef]
29. Hong, S.; Choi, J.; Chang, Y.; Mun, S. Production of High-Purity Fucose from the Seaweed of Undaria Pinnatifida through Acid-Hydrolysis and Simulated-Moving Bed Purification. *Sep. Purif. Technol.* **2019**, *213*, 133–141. [CrossRef]
30. Seidel-Morgenstern, A.; Keßler, L.C.; Kaspereit, M. New Developments in Simulated Moving Bed Chromatography. *Chem. Eng. Technol* **2008**, *31*, 826–837. [CrossRef]
31. Kim, K.-M.; Lee, J.W.; Kim, S.; Santos Da Silva, F.V.; Seidel-Morgenstern, A.; Lee, C.-H. Advanced Operating Strategies to Extend the Applications of Simulated Moving Bed Chromatography. *Chem. Eng. Technol* **2017**, *40*, 2163–2178. [CrossRef]
32. Ludemann-Hombourger, O.; Pigorini, G.; Nicoud, R.M.; Ross, D.S.; Terfloth, G. Application of the "VARICOL" Process to the Separation of the Isomers of the SB-553261 Racemate. *J. Chromatogr. A* **2002**, *947*, 59–68. [CrossRef]
33. Da Silva, A.C.; Salles, A.G.; Perna, R.F.; Correia, C.R.D.; Santana, C.C. Chromatographic Separation and Purification of Mitotane Racemate in a Varicol Multicolumn Continuous Process. *Chem. Eng. Technol* **2012**, *35*, 83–90. [CrossRef]
34. Zhang, Y.; Hidajat, K.; Ray, A.K. Multi-Objective Optimization of Simulated Moving Bed and Varicol Processes for Enantio-Separation of Racemic Pindolol. *Sep. Purif. Technol.* **2009**, *65*, 311–321. [CrossRef]
35. Schramm, H.; Kaspereit, M.; Kienle, A.; Seidel-Morgenstern, A. Improving Simulated Moving Bed Processes by Cyclic Modulation of the Feed Concentration. *Chem. Eng. Technol* **2002**, *25*, 1151–1155. [CrossRef]
36. Schramm, H.; Kaspereit, M.; Kienle, A.; Seidel-Morgenstern, A. Simulated Moving Bed Process with Cyclic Modulation of the Feed Concentration. *J. Chromatogr. A* **2003**, *1006*, 77–86. [CrossRef] [PubMed]
37. Kloppenburg, E.; Gilles, E.D. A New Concept for Operating Simulated Moving-Bed Processes. *Chem. Eng. Technol* **1999**, *22*, 813–817. [CrossRef]
38. Zhang, Z.; Morbidelli, M.; Mazzotti, M. Experimental Assessment of Powerfeed Chromatography. *AICHE J.* **2004**, *50*, 625–632. [CrossRef]
39. Bae, Y.; Lee, C. Partial-Discard Strategy for Obtaining High Purity Products Using Simulated Moving Bed Chromatography. *J. Chromatogr. A* **2006**, *1122*, 161–173. [CrossRef]
40. Kim, K.-M.; Lee, H.-H.; Lee, C.-H. Improved Performance of a Simulated Moving Bed Process by a Recycling Method in the Partial-Discard Strategy. *Ind. Eng. Chem. Res.* **2012**, *51*, 9835–9849. [CrossRef]
41. Keßler, L.C.; Seidel-Morgenstern, A. Improving Performance of Simulated Moving Bed Chromatography by Fractionation and Feed-Back of Outlet Streams. *J. Chromatogr. A* **2008**, *1207*, 55–71. [CrossRef]
42. Li, S.; Kawajiri, Y.; Raisch, J.; Seidel-Morgenstern, A. Optimization of Simulated Moving Bed Chromatography with Fractionation and Feedback: Part I. Fractionation of One Outlet. *J. Chromatogr. A* **2010**, *1217*, 5337–5348. [CrossRef]
43. Abel, S.; Mazzotti, M.; Morbidelli, M. Solvent Gradient Operation of Simulated Moving Beds I. Linear Isotherms. *J. Chromatogr. A* **2002**, *944*, 23–39. [CrossRef]
44. Wei, F.; Li, M.; Huang, F.; Chen, M.; Jiang, H.; Zhao, Y. A Novel Pseudo Simulated Moving Bed with Solvent Gradient for Ternary Separations. *J. Chromatogr. A* **2011**, *1218*, 2906–2911. [CrossRef]
45. Toumi, A.; Engell, S.; Ludemann-Hombourger, O.; Nicoud, R.M.; Bailly, M. Optimization of Simulated Moving Bed and Varicol Processes. *J. Chromatogr. A* **2003**, *1006*, 15–31. [CrossRef]
46. Lin, X.; Gong, R.; Li, J.; Li, P.; Yu, J.; Rodrigues, A.E. Enantioseparation of Racemic Aminoglutethimide Using Asynchronous Simulated Moving Bed Chromatography. *J. Chromatogr. A* **2016**, *1467*, 347–355. [CrossRef] [PubMed]
47. Sun, L.; Yang, Y.; Yu, J. Chiral Separation of Menthol Enantiomers by Simulated Moving Bed Chromatography: Mathematical Modeling and Experimental Study. *Separations* **2026**, *13*, 67. [CrossRef]
48. Zabka, M.; Minceva, M.; Sá Gomes, P.; Rodrigues, A.E. Chiral Separation of R,S-α-Tetralol by Simulated Moving Bed. *Sep. Sci. Technol.* **2008**, *43*, 727–765. [CrossRef]
49. Azevedo, D.C.S.; Rodrigues, A.E. Design of a Simulated Moving Bed in the Presence of Mass-transfer Resistances. *AICHE J.* **1999**, *45*, 956–966. [CrossRef]
50. Pais, L.S.; Loureiro, J.M.; Rodrigues, A.E. Chiral Separation by SMB Chromatography. *Sep. Purif. Technol.* **2000**, *20*, 67–77. [CrossRef]
51. Gomes, P.S.; Zabkova, M.; Zabka, M.; Minceva, M.; Rodrigues, A.E. Separation of Chiral Mixtures in Real SMB Units: The FlexSMB-LSRE®. *AICHE J.* **2010**, *56*, 125–142. [CrossRef]
52. Coelho, L.C.D.; Filho, N.M.L.; Faria, R.P.V.; Ferreira, A.F.P.; Ribeiro, A.M.; Rodrigues, A.E. Separation of Tartronic and Glyceric Acids by Simulated Moving Bed Chromatography. *J. Chromatogr. A* **2018**, *1563*, 62–70. [CrossRef]
53. Pais, L.S.; Rodrigues, A.E. Design of Simulated Moving Bed and Varicol Processes for Preparative Separations with a Low Number of Columns. *J. Chromatogr. A* **2003**, *1006*, 33–44. [CrossRef]

54. Gong, R.; Lin, X.; Li, P.; Yu, J.; Rodrigues, A.E. Experiment and Modeling for the Separation of Guaifenesin Enantiomers Using Simulated Moving Bed and Varicol Units. *J. Chromatogr. A* **2014**, *1363*, 242–249. [CrossRef]
55. Yao, C.; Tang, S.; Yao, H.; Tadé, M.O.; Xu, Y. Study on the Number of Decision Variables in Design and Optimization of Varicol Process. *Comput. Chem. Eng.* **2014**, *68*, 114–122. [CrossRef]
56. Calderón Supelano, R.; Barreto, A.G., Jr.; Andrade Neto, A.S.; Secchi, A.R. One-Step Optimization Strategy in the Simulated Moving Bed Process with Asynchronous Movement of Ports: A VariCol Case Study. *J. Chromatogr. A* **2020**, *1634*, 461672. [CrossRef]
57. Yao, C.; Jing, K.; Ling, X.; Lu, Y.; Tang, S. Application of Dodecahedron to Describe the Switching Strategies of Asynchronous Simulated-Moving-Bed. *Comput. Chem. Eng.* **2017**, *96*, 69–74. [CrossRef]
58. Mazzotti, M.; Storti, G.; Morbidelli, M. Optimal Operation of Simulated Moving Bed Units for Nonlinear Chromatographic Separations. *J. Chromatogr. A* **1997**, *769*, 3–24. [CrossRef]
59. Ribeiro, A.E.; Gomes, P.S.; Pais, L.S.; Rodrigues, A.E. Chiral Separation of Flurbiprofen Enantiomers by Preparative and Simulated Moving Bed Chromatography. *Chirality* **2011**, *23*, 602–611. [CrossRef]
60. Toumi, A.; Hanisch, F.; Engell, S. Optimal Operation of Continuous Chromatographic Processes: Mathematical Optimization of the VARICOL Process. *Ind. Eng. Chem. Res.* **2002**, *41*, 4328–4337. [CrossRef]
61. Zhong, Y.J.; Guo, D.; Fan, J.; Ruan, L.J.; Gao, R.Q.; Zhang, W.G. HPLC Enantioseparation of Menthol with Non-Ultraviolet Detectors and Effect of Chromatographic Conditions. *Chromatographia* **2018**, *81*, 871–879. [CrossRef]